ADVANCED ENERGY MATERIALS
www.advenergymat.de

Ni and Co Segregations on Selective Surface Facets and Rational Design of Layered Lithium Transition-Metal Oxide Cathodes

Pengfei Yan, Jianming Zheng, Jiaxin Zheng, Zhiguo Wang, Gaofeng Teng, Saravanan Kuppan, Jie Xiao, Guoying Chen, Feng Pan, Ji-Guang Zhang, and Chong-Min Wang**

The chemical processes occurring on the surface of cathode materials during battery cycling play a crucial role in determining battery's performance. However, the understanding of such surface chemistry is far from clear due to the complexity of redox chemistry during battery charge/discharge. Through intensive aberration corrected STEM investigation on ten layered oxide cathode materials, two important findings on the pristine oxides are reported. First, Ni and Co show strong plane selectivity when building up their respective surface segregation layers (SSLs). Specifically, Ni-SSL is exclusively developed on $(200)_m$ facet in Li–Mn-rich oxides (monoclinic C2/m symmetry) and on $(012)_h$ facet in Mn–Ni equally rich oxides (hexagonal R-3m symmetry), while Co-SSL has a strong preference to $(20\text{–}2)_m$ plane with minimal Co-SSL also developed on some other planes in Li–Mn-rich cathodes. Structurally, Ni-SSLs tend to form spinel-like lattice while Co-SSLs are in a rock-salt-like structure. Second, by increasing Ni concentration in these layered oxides, Ni and Co SSLs can be suppressed and even eliminated. The findings indicate that Ni and Co SSLs are tunable through controlling particle morphology and oxide composition, which opens up a new way for future rational design and synthesis of cathode materials.

1. Introduction

In order to achieve a wide application of lithium-ion batteries (LIBs) in the portable device market, especially for electrical vehicles, the performances of LIBs need to be further improved. The performance metrics include energy density, cycle stability, rate capability, and safety, in all of which cathode component plays a critical role.[1–5] Often as the sole Li source in LIB cells, the amount of Li cations can be reversibly extracted and inserted into the cathode determines battery's capacity. For these reasons, developing advanced cathode materials for the next-generation LIBs has been one of the main efforts in the past decades.[6–16] Categorized by crystal structure, the cathode materials under intensive investigation include layered compounds ($LiMO_2$ (M = Mn, Ni, Co), Li_2MnO_3, and their compounds), spinel compounds (LiM_2O_4, M = Mn, Ni), and olivine compounds ($LiMPO_4$, M = Fe, Mn, Ni, Co, etc.), among which layered compounds is most promising due to their high energy density originated from a high operating voltage and a large reversible capacity. However, significant gap between theoretical and practical capacity still exists which mandates further optimization and development of these layered oxide cathodes.

In order to obtain superior cathode materials, most efforts have focused on optimizing materials' chemical compositions that engineer particle's bulk properties. Layered compounds with a range of compositions have been synthesized and evaluated, which led to the commercialization of $LiNi_{1/3}Mn_{1/3}Co_{1/3}O_2$ (NMC333) and $LiNi_{0.4}Mn_{0.4}Co_{0.2}O_2$ (NMC442) cathode materials. On the other hand, when cathode materials are subjected to battery cycling, material degradation often initiates from the surface layer, as evidenced by recent characterization studies.[17–22] For example, a surface reconstruction layer (SRL) was frequently observed on cathode particle surface after battery cycling, which was believed to act as a barrier for Li-ion transport and thus contribute to battery' high polarization and poor rate capability.[17–21,23–25] Moreover, such SRL keeps growing from particle surface into inner bulk as battery cycling continues, which is believed to contribute to battery's capacity and voltage decay. The nature of the surface layer also influences the solid electrolyte interphase (SEI),[21,26–28] particle corrosion[22,29,30] and

Dr. P. Yan, Dr. C.-M. Wang
Environmental Molecular Sciences Laboratory
Pacific Northwest National Laboratory
902 Battelle Boulevard, Richland, WA 99352, USA
E-mail: Chongmin.wang@pnnl.gov
Dr. J. Zheng, Dr. J. Xiao, Dr. J.-G. Zhang
Energy and Environmental Directorate
Pacific Northwest National Laboratory
902 Battelle Boulevard, Richland, WA 99352, USA
E-mail: Jiguang.zhang@pnnl.gov
Dr. J. Zheng, G. Teng, Dr. F. Pan
School of Advanced Materials
Peking University
Shenzhen Graduate School
Shenzhen 518055, China
Dr. Z. Wang
Department of Applied Physics
University of Electronic Science and Technology of China
Chengdu 610054, China
Dr. S. Kuppan, Dr. G. Chen
Energy Storage and Distributed Resources Division
Lawrence Berkeley National Laboratory
Berkeley, CA 94720, USA

DOI: 10.1002/aenm.201502455

side reactions with the electrolyte,[26,28,29] all of which are critical to LIB performance. To this end, much effort has been directed to optimize surface chemistry and stabilize surface structure using coating techniques and surface treatments.[31–36]

Little attention was paid to the surface structure of pristine cathode materials until in recent years.[37,38] Several transmission electron microscopy (TEM) studies revealed that Ni tends to segregate on certain surface facets in Li–Mn-rich (LMR) oxides which results in structural and chemical modifications of the surface layer.[18,38–40] As aforementioned, such surface modification can be expected to affect the performance of cathode materials. The fundamental understanding on the surface modification layer, however, is largely nonexistent as systematic investigation on surface segregation has not been carried out. In this work, we investigated several layered cathode materials with different compositions using scanning TEM equipped with a high angle annular dark field (HAADF) detector, a Gatan energy filter system and an advanced energy dispersive X-ray spectrometer (EDS) with high collection efficiency. We found that the surface segregation of Ni and Co shows distinctive plane selectivity and composition dependence. The modification on surface layer's structure and chemical composition were investigated in a systematic way. This work provides fundamental understanding on cathode surface layer and more importantly, the findings revealed in this work can guide rational design and synthesis of advanced cathode materials for better battery performance.

2. Results and Discussion

2.1. Distinctive Surface Segregation of Ni and Co in Monoclinic LMR Cathodes

Based on collective observations of a large number of LMR particles, we found that for $Li_{1.2}Ni_{0.13}Co_{0.13}Mn_{0.54}O_2$ and $Li_{1.2}Ni_{0.2}Mn_{0.6}O_2$,

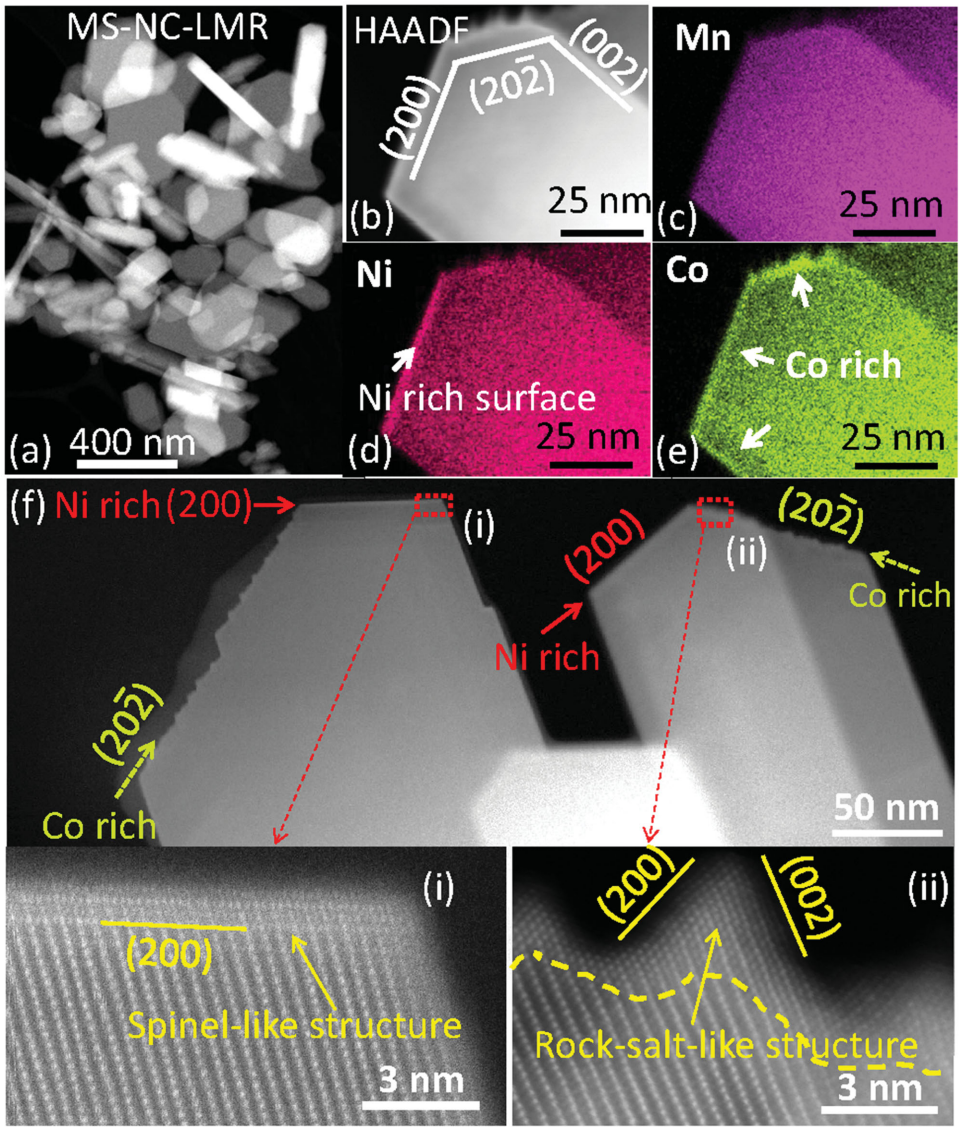

Figure 1. MS-NC-LMR cathode. a) Low-magnification STEM-HAADF image showing the plate-shape particles, b–e) EDS mapping on one particle, and f) well-defined particles and surface structure modifications due to Ni and Co enrichment.

both Ni and Co are prone to segregation to the particle surfaces. However, Ni and Co segregate at distinctively different surface planes: Ni is exclusively segregated at the $(200)_m$ surface (the subscript m indicate monoclinic lattice), while Co predominately enriched on the $(20–2)_m$ surface and slight enrichment on $(200)_m$ and $(002)_m$ facets was also observed. These phenomena have been observed on the particles synthesized by different methods with different morphological features as described below. Three LMR oxides were studied, namely molten-salt method prepared $Li_{1.2}Ni_{0.13}Co_{0.13}Mn_{0.54}O_2$ (MS-NC-LMR), coprecipitation method prepared $Li_{1.2}Ni_{0.13}Co_{0.13}Mn_{0.54}O_2$ (CP-NC-LMR) and $Li_{1.2}Ni_{0.2}Mn_{0.6}O_2$ (20N-LMR). The MS-NC-LMR oxide particles are plate-shaped with well-defined surface facets, and the large plate surfaces were identified as the $(002)_m$ plane (**Figure 1**a). Figure 1b–e shows EDS elemental mapping on a particle that was viewed along $[010]_m$ zone axis. From the X-ray signal intensity, we can directly see a Ni-rich surface layer on the $(200)_m$ facet, strong Co-rich surface layer on $(20–2)_m$ facet and a slight Co-rich surface layer on $(200)_m$ and $(002)_m$ facets. EDS mappings on multiple MS-NC-LMR oxide particles indicate that Ni exclusively segregates to the $(200)_m$ facet, while Co has a strong preference to segregate on $(20–2)_m$ plane with some other surface planes showing slight Co-enrichment (more examples can be found in Figure S1 in the Supporting Information). Quantitative EDS measurements were conducted on both Ni-rich and Co-rich surface layer, i.e., $(200)_m$ and $(20–2)_m$ facets, respectively. Although slightly different Ni/Co/Mn ratio values were observed on different particles, the average Ni/Co/Mn ratio value for the Ni-rich surface layers is ≈4:2:5, while the average Ni/Co/Mn ratio value of Co-enriched

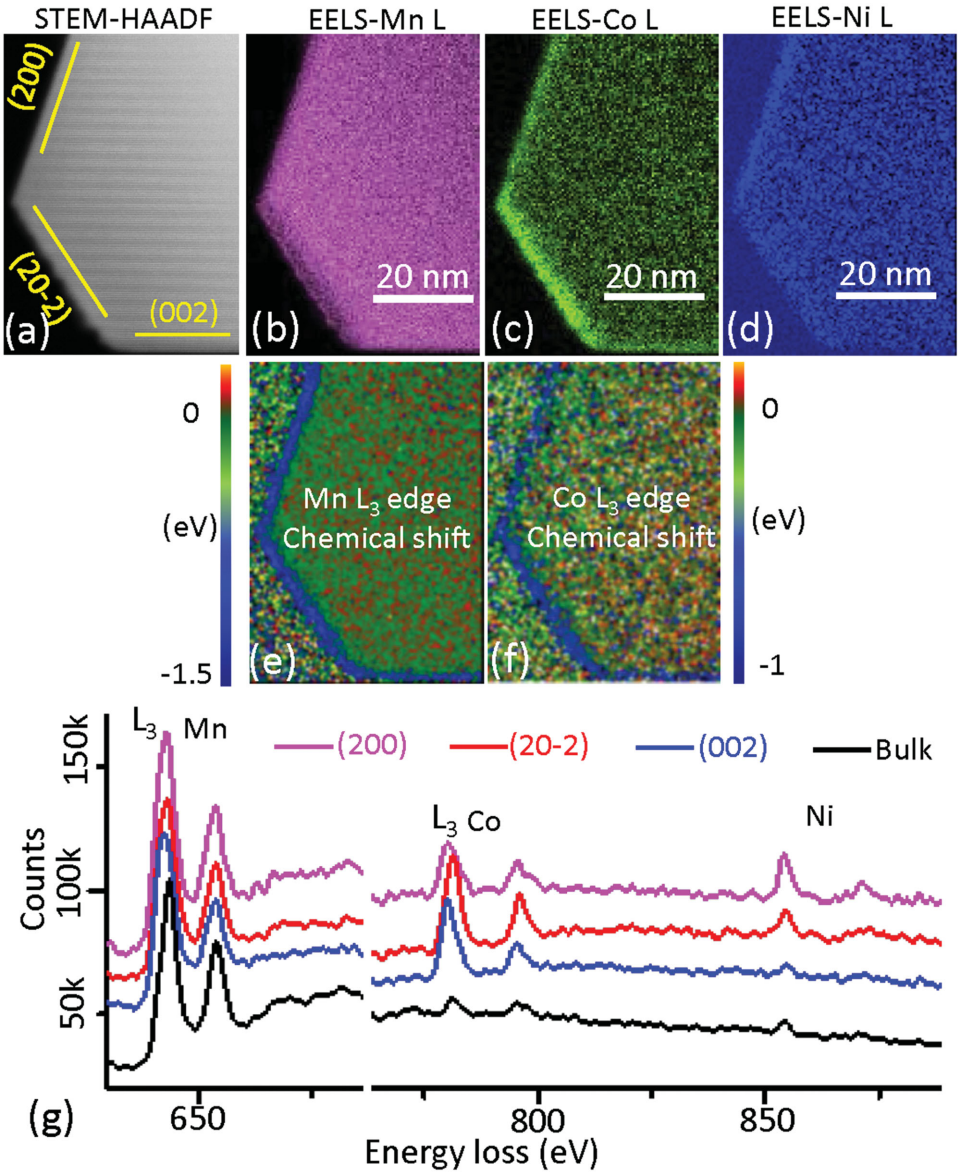

Figure 2. a–d) STEM-EELS mapping of an MS-NC-LMR particle, e) Mn L_3 edge chemical shift map, f) Co L_3 edge chemical shift map, and g) EELS spectra from (200), (20–2), (002) surfaces and inner bulk, showing chemical shift and peak intensity change due to Ni/Co surface segregation.

$(20–2)_m$ surface is ≈1:2:2. The bulk ratio of Ni/Co/Mn in the sample is 1:1:4. Along with the Ni and Co enrichment on these surfaces, the lattice structure was modified on both $(200)_m$ and $(20–2)_m$ surfaces. As shown in Figure 1f, a spinel-like structure was developed on Ni-rich surface segregation layer (SSL), while rock-salt-like structure was developed on Co-rich SSL. Moreover, the Ni-rich SSL has an atomic level flatness surface ((i) in Figure 1f) while strong Co-rich SSL develops a zigzag shape surface along $(20–2)_m$ plane (see (ii) in Figure 1f). High-resolution lattice images revealed that the zigzag surface is, in fact, due to the formation of micro surface steps. As illustrated in (ii) of Figure 1f, the surface steps are terminated by $(200)_m$ and $(002)_m$ planes. Thus, the MS-NC-LMR oxide tends to have $(200)_m$ and $(002)_m$ planes as the exposed surfaces. Structurally, these two planes are the most closed packed ones; chemically, these two planes are stacked alternatively by pure cations (TM and Li) and pure anions (oxygen).

The STEM-EELS elemental maps (**Figure 2**a–d) show Ni/Co surface segregation consistent with the results from EDS mapping (Figure 1). Moreover, EELS mapping allows us to extract TM valence state information based on either L-edge energy shift (so-called chemical shift) or L_3/L_2 white-line intensity ratios. As shown in Figure 2e,f, a clear chemical shift was observed on the surface for both Mn L_3 edge and Co L_3 edge as compared to that of the bulk, indicating reduced valence state of Mn and Co in the surface layer. Furthermore, the reduced layer overlaps with the Ni and Co enriched layer on $(200)_m$ and $(20–2)_m$ surfaces, indicating that surface transition metal enrichment and reduction are closely related, which is further associated with the structural modification occurred on SSLs. Sample EELS spectra from the three surfaces and bulk are shown in Figure 2g, which clearly shows chemical shift of Mn and Co as well as TM concentration change (peak intensity change).

Different synthesis procedure often yields significantly different particle morphology and therefore dominance of different surface facets. The observation of Ni and Co segregation on selective surface planes holds true on distinctively different morphologies. As

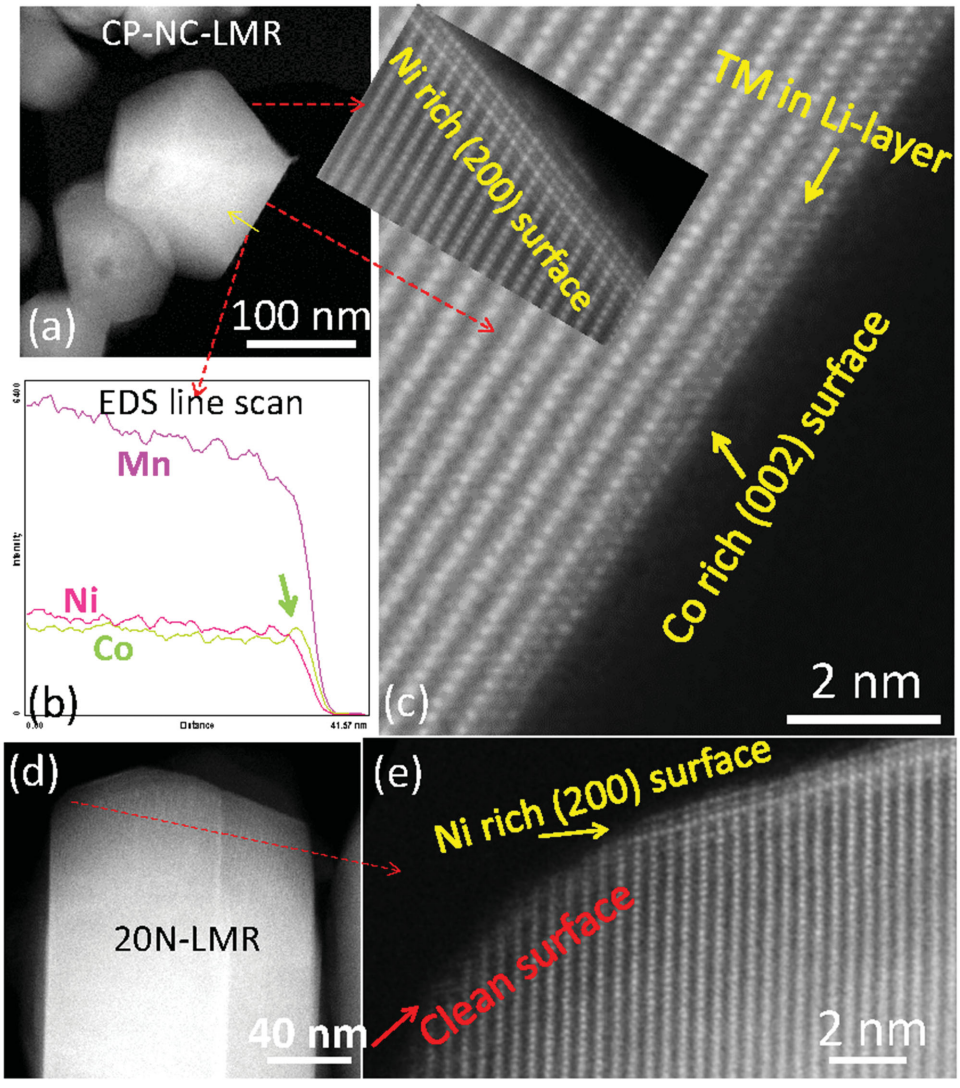

Figure 3. a–c) CP-NC-LMR cathode. a) Particle morphology, b) EDS line scan across the $(002)_m$ surface layer, c) high-magnification STEM-HAADF images to show (i) Ni-segregation surface layer and (ii) Co segregation surface layer. d,e) STEM-HAADF images of 20N-LMR.

shown in **Figure 3**a, CP-NC-LMR particles made by the coprecipitation method are not plate-shaped and their particle surfaces are not as well-defined as those of MS-NC-LMR. For CP-NC-LMR, only $(200)_m$ and $(002)_m$ surface facets could be identified as the $(20–2)_m$ facet was not expressed. For both MS-NC-LMR and CP-NC-LMR particles, the $(200)_m$ planes are significantly enriched with Ni and slightly enriched with Co, as shown in Figure 3b,c. The absence of $(20–2)_m$ terminating planes in the CP-NC-LMR leads to the elimination of the Co segregation on the surface, contrasting the observation on MS-NC-LMR particle. In other words, by eliminating the $(20–2)_m$ surface facets, CP method can eliminate the strong Co-rich surface layer. Similarly, Ni segregation can be eliminated by removing the $(200)_m$ facet. Figure 3e shows that once the surface deviates from $(200)_m$ plane, Ni-rich layer disappears as indicated by the red arrow.

In order to compare LMR oxides with different compositions, we synthesized 20N-LMR by the CP method. Ni-rich surface layer was also observed on the $(200)_m$ surface facet in this sample (Figure 3d,e). Previous study on another LMR oxide ($Li_{1.2}Ni_{0.175}Mn_{0.525}Co_{0.1}O_2$) confirmed the presence of Ni enriched $(200)_m$ surface, either synthesized by the CP method[40] or by the sol–gel synthesis method.[16] In **Figure 4**, we also

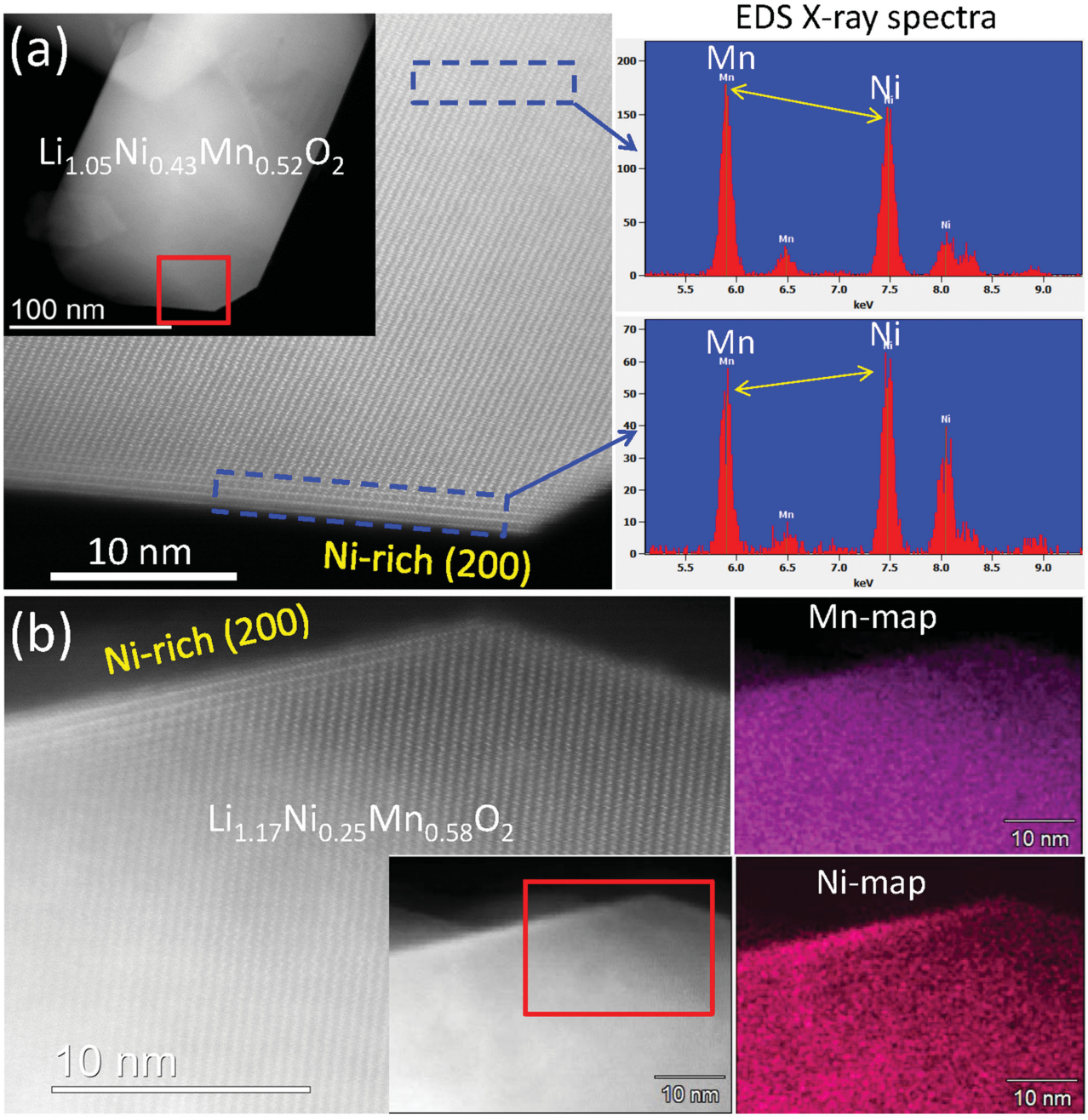

Figure 4. Formation of Ni-rich SSL on LMR cathodes with a chemical composition of a) $Li_{1.05}Ni_{0.43}Mn_{0.52}O_2$ and b) $Li_{1.17}Ni_{0.25}Mn_{0.58}O_2$ (note the different Li content).

observed different Li content LMR oxides, $Li_{1.05}Ni_{0.43}Mn_{0.52}O_2$ and $Li_{1.17}Ni_{0.25}Mn_{0.58}O_2$. Ni-enriched $(200)_m$ surface layers were also verified to adopt spinel-like structure. We therefore conclude that Ni exclusively segregates to the $(200)_m$ surface in LMR cathodes regardless compositions and synthesis methods.

Combined with Co surface segregation behavior, we report that for LMR cathodes there is a strong plane selectivity for both Ni and Co surface segregation. This important insight indicates that it is possible to adjust synthesis conditions and/or methods to minimize or maximize the surface effect that may ultimately leads to optimized materials for LIBs. Prior work has demonstrated in some degrees that Ni segregation is closely related to the battery capacity fading in the case of $Li_{1.2}Ni_{0.2}Mn_{0.6}O_2$,[16] but further detailed study is needed to clarify the roles of such SSLs in battery's performance.

2.2. Composition Effect on Ni and Co Surface Segregation

With decreasing Li content and increasing Ni content, we observed distinctive changes of Ni and Co surface segregation behavior in the layered oxides with R-3m symmetry. Two Mn–Ni equally rich cathodes synthesized by CP method, $LiNi_{0.4}Mn_{0.4}Co_{0.2}O_2$ (NMC442) and $LiNi_{0.5}Mn_{0.5}O_2$ (NM55), were investigated by STEM-HAADF imaging and EDS analysis, and the results are shown in **Figure 5**. By tilting the two samples to $[100]_h$ zone axis, we found only slightly enriched Ni-SSLs on the $(012)_h$ surface plane which is equivalent to LMR $(200)_m$ surface in terms of lattice configuration. The plane selectivity of Ni surface segregation remains even with the changes in crystal structure and/or chemical composition. Even though Ni enrichment level was significantly lower than that in LMR oxides, evidenced by the EDS line scans in Figure 5b,d and EDS mapping in Figure S2 (Supporting Information), the modification from the original layered structure to a spinel-like structure still occurred (Figure 5). On the other hand, we noted that Co surface enrichment was completely eliminated in NMC442.

For Ni-rich layered cathode materials, such as NMC622, NMC811, and NCA, EDS measurements cannot detect any Ni-rich and/or Co-rich layer on their surface, indicating no transition metal segregation occurring on their surfaces. Examples are given in **Figure 6**a–c, by tilting the particle to $[100]_h$ zone axis, edge on $(012)_h$ surfaces show no Ni enrichment. However, high-resolution STEM-HAADF imaging indicates that such Ni-rich oxides' surface layers have been transformed into a rock-salt-like structure, indicating the surface structure of Ni-rich cathodes is not stable. Figure 6d shows a similar rock-salt-like structure on the surfaces of Ni-rich particles with different compositions.

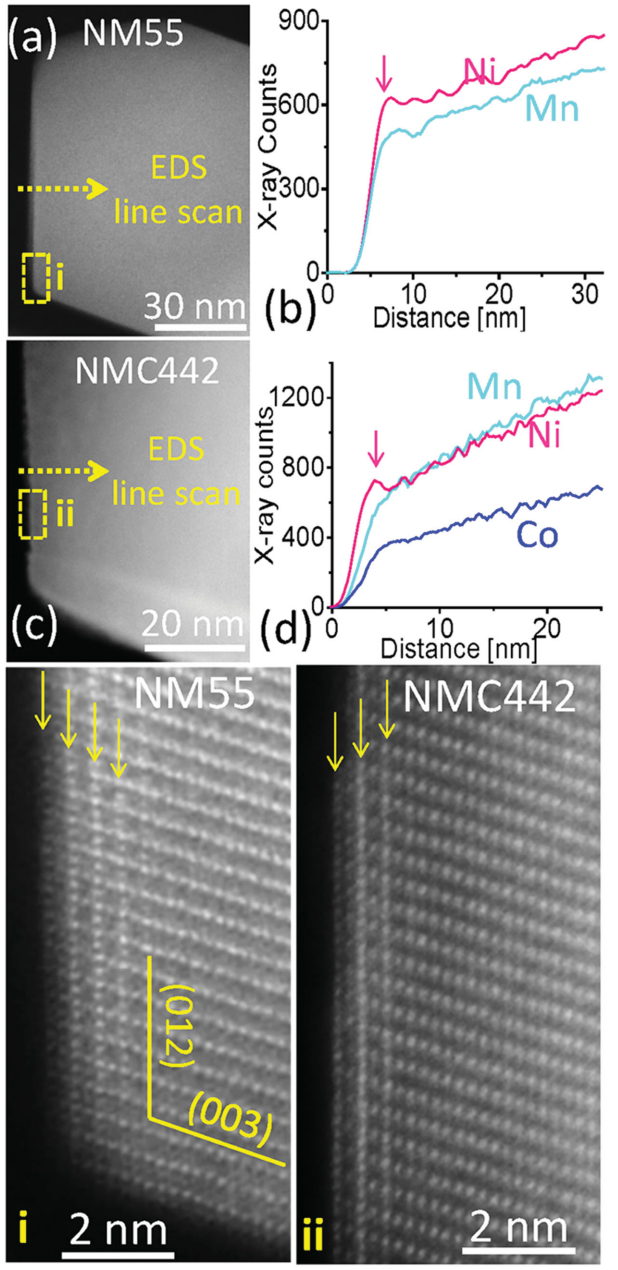

Figure 5. Chemical composition and lattice structure of Ni segregation surface layer in a,b) NM55 sample and c,d) NMC442 sample. Parts (b) and (d) are EDS line scans in (a) and (c), respectively. Lattice structure of Ni-SSLs in (a) and (b) are shown as STEM-HAADF images areas (i) and (ii), respectively.

2.3. General Discussion

A schematic diagram is shown in **Figure 7** to illustrate the plane selectivity and composition dependence of the TM SSL in layered oxides. In terms of plane selectivity, Ni and Co show strong preference to certain surface plane in LMR cathodes. Typically, as illustrated in the molten salt-LMR, Ni exclusively segregates to $(200)_m$ facet and Co shows strong preference to $(20–2)_m$ facet. In the case of CP-LMR, Co-SSL was eliminated along with the disappearance of the $(20–2)_m$ surface plane on the particles. In terms of composition dependence, we found that increasing Ni concentration can significantly suppress both Ni and Co surface segregation. For Ni-rich layered cathodes, both Ni and Co-SSLs can be completely avoided. Accompanied with material's composition change, structural change was also observed on the surface layer, as depicted in Figure 7.

The three common TMs in layered lithium transition metal oxides, Ni, Co, and Mn, have different chemical and physical

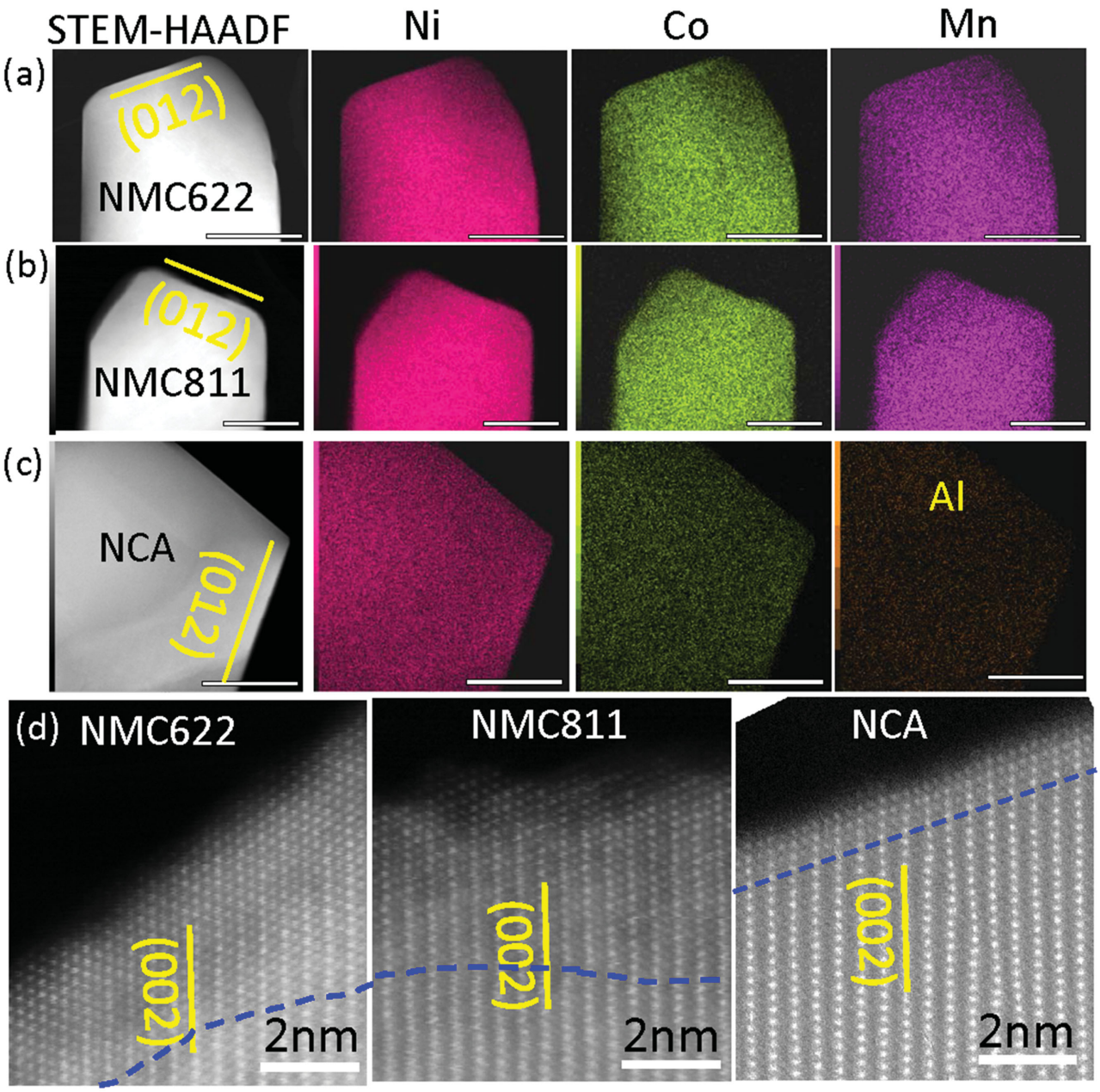

Figure 6. a–c) EDS mapping and d) surface layer lattice structure of three Ni-rich cathodes NMC622, NMC811, and NCA. Scale bars are 100 nm in (a–c).

characteristics. In order to obtain superior ternary Ni–Co–Mn layered cathodes, a deep understanding on how each TM affects material's performance is crucial. Previous investigation indicates that all TM have their advantages and drawbacks.[41–43] For example, Ni and Co are efficient redox centers enabling Li-ion intercalation and deintercalation but their high mobility degrades material's cycle stability. Mn^{4+} has high chemical stability which can stabilize the layered structure, but it has poor redox behavior because once Mn^{4+} is reduced to Mn^{3+} and Mn^{2+}, the layered lattice structure is no longer stable and lattice reconstruction occurs due to the well-known Jahn–Teller effect[44,45] and increased cation mobility.[46,47] Increasing Co content can improve rate capability but it brings in cost and safety issues. Increasing Ni content can lead to better cycle stability but rate capability decreases due to a high-level interlayer Li/Ni mixing.[48–50] Therefore, the composition optimization of ternary Ni–Co–Mn oxide involves a complex trade-off between the advantages and drawbacks of each transition metal. Our current work, aiming at surface structure and chemistry in pristine layered cathodes, provides systematic characterizations of Ni and Co surface segregation effect.

Though the effect of Ni/Co SSL on battery performance is not fully clear, we still anticipate some possible impacts. First, the Ni/Co SSL may block Li-ion transportation, since following the Ni and Co surface segregation, the original layered structure at the surface has been modified into spinel structure (Ni-SSL) or

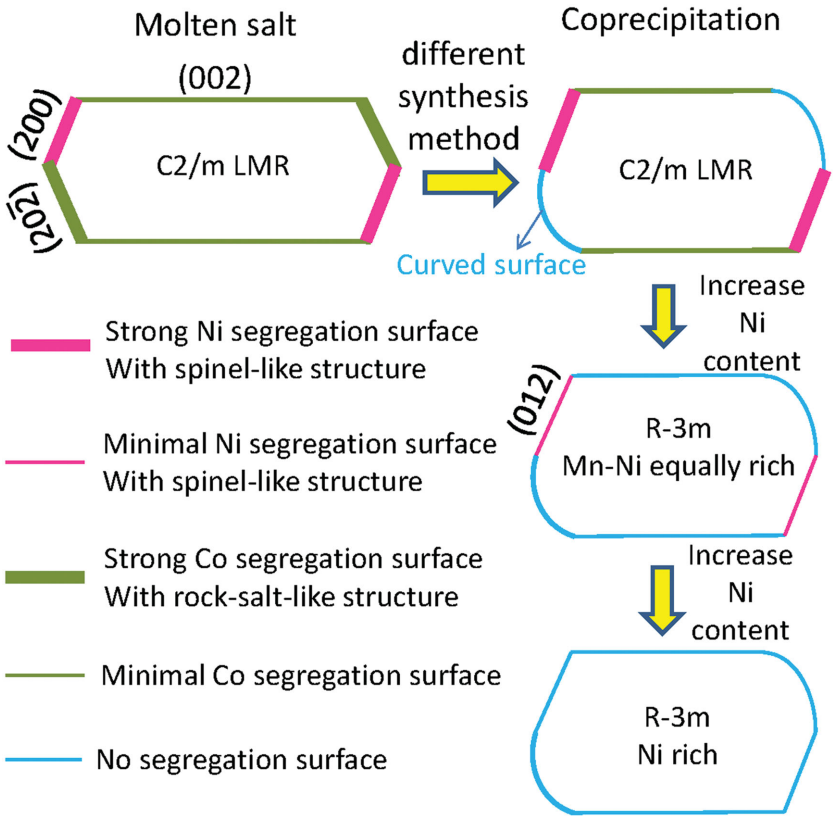

Figure 7. Schematic diagram to show the plane selectivity of Ni and Co SSLs and their composition dependence.

rock salt structure (Co-SSL), which will result in poor cycle rate and high polarization. Second, due to the high stability of spinel structure, Ni-SSL may act as a protective surface layer against surface corrosion and structure degradation, which can enhance cathode stability during the cycling of the battery. In contrast, the Co-SSL with a rock salt structure may be not as stable as Ni-SSL and repeated battery cycling may result in Co dissolution in the electrolyte. Thus, in terms of cathode stability, Co-SSL is believed to play solely a detrimental role while Ni-SSL may be utilized to increase cathode stability. Apparently, more detailed study is needed to quantitatively clarify the effect of such a SSL on battery performance in order to guide cathode synthesis in terms of controlling surface structure and chemistry.

3. Conclusions

Elemental segregation and structural modification of surface layer in ten pristine layered lithium transition metal oxide cathodes were investigated by STEM structural imaging and EDS/EELS chemical mapping. On one hand, Ni and Co show distinctive plane selectivity while forming SSLs on particle surface as evidenced in several LMR oxides regardless of the synthesis methods: Ni exclusively segregates to $(200)_m$ plane and Co prefer to $(20–2)_m$ plane. On the other hand, such Ni and Co SSLs show composition dependence of cathode materials. We found that both Ni and Co SSLs can be eliminated by increasing Ni concentration to Ni-rich layered oxides. These findings indicate that Ni and Co SSLs are adjustable through two strategies. One is by controlling surface morphology and the other one is by controlling material compositions. Structurally, we also found Ni-SSLs tend to form a spinel-like structure while Co-SSLs form a rock-salt-like structure. In Ni-rich cathodes, surface layers were found to transform into rock-salt-like structure even without any transition metal segregation. The systematical investigation in this work will facilitate our fundamental understanding on Ni–Co–Mn-based layered cathode oxides and provide valuable guidelines for cathode material design and synthesis.

4. Experimental Section

Material Synthesis: $Li_{1.2}Ni_{0.13}Co_{0.13}Mn_{0.54}O_2$ (MS-NC-LMR) was synthesized by using a molten salt method as described in a previous publication.[51] $Li_{1.2}Ni_{0.13}Co_{0.13}Mn_{0.54}O_2$ (CP-NC-LMR), $Li_{1.2}Ni_{0.2}Mn_{0.6}O_2$ (20N-LMR), $LiNi_{0.5}Mn_{0.5}O_2$ (NM55), $LiNi_{0.6}Co_{0.2}Mn_{0.2}O_2$ (NMC622), and $LiNi_{0.8}Co_{0.1}Mn_{0.1}O_2$ (NMC811) were synthesized via a coprecipitation method. The detailed description of the synthesis procedure was reported in prior publications.[17,42] $Li_{1.05}Ni_{0.43}Mn_{0.52}O_2$ and $Li_{1.17}Ni_{0.25}Mn_{0.58}O_2$ were synthesized by hydrothermal assisted method. $LiNi_{0.4}Co_{0.2}Mn_{0.4}O_2$ (NMC442) and $LiNi_{0.8}Co_{0.15}Al_{0.05}O_2$ (NCA)) are commercially available materials manufactured by TODA KOGYO company (provided by CAMP Facility at Argonne National Laboratory).

TEM Characterizations: The ten layered oxides were investigated by JEOL JEM-ARM200CF microscope, which is operated at 200 kV. This microscope is equipped with a probe spherical aberration corrector, Gantan Quantum EELS system and a JEOL SDD-detector with a 100 mm^2 X-ray sensor, enabling sub-angstrom resolution in STEM mode with excellent noise-to-signal ratio and high-efficient X-ray collection that is ten times faster than the traditional detector. For the STEM-HAADF imaging, the inner and outer collection angles of annular dark field detector were set at 68 and 280 mrad, respectively. For EDS mapping, signals were collected by scanning the same region with multiple times at a dwell time of 0.1ms and electron probe current ≈100 pA. The EDS line scan signal was extracted from corresponding mapping results. The EDS data were collected and processed by using Analysis Station 3.8.0.52 (JEOL Engineering Co., Ltd). For STEM-EELS mapping, the dwell time is 0.01s per pixel and collection angle is 82.6 mrad.

Supporting Information

Supporting Information is available from the Wiley Online Library or from the author.

Acknowledgements

P.Y. and J.Z. contributed equally to this work. This work was supported by the Assistant Secretary for Energy Efficiency and Renewable Energy, Office of Vehicle Technologies of the U.S. Department of Energy under

Contract No. DE-AC02-05CH11231, Subcontract No. 6951379 under the Batteries for Advanced Battery Materials Research (BMR). The work was conducted in the William R. Wiley Environmental Molecular Sciences Laboratory (EMSL), a national scientific user facility sponsored by DOE's Office of Biological and Environmental Research and located at PNNL. PNNL is operated by Battelle for the Department of Energy under Contract DE-AC05-76RLO1830. Z.W. was supported by the National Natural Science Foundation of China (Grant No. 11474047).

Received: December 10, 2015
Revised: January 4, 2016
Published online:

[1] M. S. Whittingham, *Chem. Rev.* **2004**, *104*, 4271.
[2] M. Hu, X. L. Pang, Z. Zhou, *J. Power Sources* **2013**, *237*, 229.
[3] M. Gu, Y. Li, X. Li, S. Hu, X. Zhang, W. Xu, S. Thevuthasan, D. R. Baer, J. G. Zhang, J. Liu, C. M. Wang, *ACS Nano* **2012**, *6*, 8439.
[4] A. Manthiram, *J. Phys. Chem. Lett.* **2011**, *2*, 176.
[5] R. Marom, S. F. Amalraj, N. Leifer, D. Jacob, D. Aurbach, *J. Mater. Chem.* **2011**, *21*, 9938.
[6] Y.-K. Sun, Z. Chen, H.-J. Noh, D.-J. Lee, H.-G. Jung, Y. Ren, S. Wang, C. S. Yoon, S.-T. Myung, K. Amine, *Nat. Mater.* **2012**, *11*, 942.
[7] G. Ceder, Y. M. Chiang, D. R. Sadoway, M. K. Aydinol, Y. I. Jang, B. Huang, *Nature* **1998**, *392*, 694.
[8] J. M. Tarascon, M. Armand, *Nature* **2001**, *414*, 359.
[9] K. Kang, Y. S. Meng, J. Breger, C. P. Grey, G. Ceder, *Science* **2006**, *311*, 977.
[10] J. Lee, A. Urban, X. Li, D. Su, G. Hautier, G. Ceder, *Science* **2014**, *343*, 519.
[11] M. M. Thackeray, C. S. Johnson, J. T. Vaughey, N. Li, S. A. Hackney, *J. Mater. Chem.* **2005**, *15*, 2257.
[12] J. R. Croy, D. Kim, M. Balasubramanian, K. Gallagher, S.-H. Kang, M. M. Thackeray, *J. Electrochem. Soc.* **2012**, *159*, A781.
[13] Y. K. Sun, S. T. Myung, B. C. Park, J. Prakash, I. Belharouak, K. Amine, *Nat. Mater.* **2009**, *8*, 320.
[14] Z. H. Lu, L. Y. Beaulieu, R. A. Donaberger, C. L. Thomas, J. R. Dahn, *J. Electrochem. Soc.* **2002**, *149*, A778.
[15] J. Li, J. Camardese, R. Shunmugasundaram, S. Glazier, Z. Lu, J. R. Dahn, *Chem. Mater.* **2015**, *27*, 3366.
[16] J. Zheng, M. Gu, A. Genc, J. Xiao, P. Xu, X. Chen, Z. Zhu, W. Zhao, L. Pullan, C. M. Wang, J. G. Zhang, *Nano Lett.* **2014**, *14*, 2628.
[17] P. Yan, A. Nie, J. Zheng, Y. Zhou, D. Lu, X. Zhang, R. Xu, I. Belharouak, X. Zu, J. Xiao, K. Amine, J. Liu, F. Gao, R. Shahbazian-Yassar, J. G. Zhang, C. M. Wang, *Nano Lett.* **2015**, *15*, 514.
[18] P. Yan, L. Xiao, J. Zheng, Y. Zhou, Y. He, X. Zu, S. X. Mao, J. Xiao, F. Gao, J.-G. Zhang, C.-M. Wang, *Chem. Mater.* **2015**, *27*, 975.
[19] A. Boulineau, L. Simonin, J. F. Colin, C. Bourbon, S. Patoux, *Nano Lett.* **2013**, *13*, 3857.
[20] F. Lin, I. M. Markus, D. Nordlund, T. C. Weng, M. D. Asta, H. L. Xin, M. M. Doeff, *Nat. Commun.* **2014**, *5*, 3529.
[21] B. Xu, C. R. Fell, M. F. Chi, Y. S. Meng, *Energy Environ. Sci.* **2011**, *4*, 2223.
[22] J. Zheng, M. Gu, J. Xiao, P. Zuo, C. Wang, J. G. Zhang, *Nano Lett.* **2013**, *13*, 3824.
[23] J. Zheng, P. Xu, M. Gu, J. Xiao, N. D. Browning, P. Yan, C. M. Wang, J.-G. Zhang, *Chem. Mater.* **2015**, *27*, 1381.
[24] D. P. Abraham, R. D. Twesten, M. Balasubramanian, I. Petrov, J. McBreen, K. Amine, *Electrochem. Commun.* **2002**, *4*, 620.
[25] L. Gu, D. Xiao, Y.-S. Hu, H. Li, Y. Ikuhara, *Adv. Mater.* **2015**, *27*, 2134.
[26] M. B. Pinson, M. Z. Bazant, *J. Electrochem. Soc.* **2013**, *160*, A243.
[27] K. J. Carroll, D. Qian, C. Fell, S. Calvin, G. M. Veith, M. Chi, L. Baggetto, Y. S. Meng, *Phys. Chem. Chem. Phys.* **2013**, *15*, 11128.
[28] P. Yang, J. Zheng, S. Kuppan, Q. Li, D. Lv, J. Xiao, G. Chen, J.-G. Zhang, C.-M. Wang, *Chem. Mater.* **2015**, *27*, 7447.
[29] P. Arora, R. E. White, M. Doyle, *J. Electrochem. Soc.* **1998**, *145*, 3647.
[30] S. Muto, Y. Sasano, K. Tatsumi, T. Sasaki, K. Horibuchi, Y. Takeuchi, Y. Ukyo, *J. Electrochem. Soc.* **2009**, *156*, A371.
[31] S.-H. Kang, M. M. Thackeray, *Electrochem. Commun.* **2009**, *11*, 748.
[32] L. Li, Y. L. Chang, H. Xia, B. H. Song, J. R. Yang, K. S. Lee, L. Lu, *Solid State Ionics* **2014**, *264*, 36.
[33] J. Zheng, M. Gu, J. Xiao, B. J. Polzin, P. Yan, X. Chen, C. M. Wang, J.-G. Zhang, *Chem. Mater.* **2014**, *26*, 6320.
[34] Y. Wu, A. Manthiram, *Electrochem. Solid-State Lett.* **2006**, *9*, A221.
[35] Y.-K. Sun, M.-J. Lee, C. S. Yoon, J. Hassoun, K. Amine, B. Scrosati, *Adv. Mater.* **2012**, *24*, 1192.
[36] W. Liu, P. Oh, X. Liu, S. Myeong, W. Cho, J. Cho, *Adv. Energy Mater.* **2015**, *5*, 1500274.
[37] A. K. Shukla, Q. M. Ramasse, C. Ophus, H. Duncan, F. Hage, G. Chen, *Nat. Commun.* **2015**, *6*, 8711.
[38] M. Gu, I. Belharouak, A. Genc, Z. Wang, D. Wang, K. Amine, F. Gao, G. Zhou, S. Thevuthasan, D. R. Baer, J. G. Zhang, N. D. Browning, J. Liu, C. M. Wang, *Nano Lett.* **2012**, *12*, 5186.
[39] M. Gu, A. Genc, I. Belharouak, D. P. Wang, K. Amine, S. Thevuthasan, D. R. Baer, J. G. Zhang, N. D. Browning, J. Liu, C. M. Wang, *Chem. Mater.* **2013**, *25*, 2319.
[40] H. Dixit, W. Zhou, J. C. Idrobo, J. Nanda, V. R. Cooper, *ACS Nano* **2014**, *8*, 12710.
[41] C. Zhao, X. Wang, X. Liu, H. Zhang, Q. Shen, *ACS Appl. Mater. Interfaces* **2014**, *6*, 2386.
[42] J. Zheng, W. H. Kan, A. Manthiram, *ACS Appl. Mater. Interfaces* **2015**, *7*, 6926.
[43] D. Kim, J. R. Croy, M. M. Thackeray, *Electrochem. Commun.* **2013**, *36*, 103.
[44] X. Li, X. H. Ma, D. Su, L. Liu, R. Chisnell, S. P. Ong, H. L. Chen, A. Toumar, J. C. Idrobo, Y. C. Lei, J. M. Bai, F. Wang, J. W. Lynn, Y. S. Lee, G. Ceder, *Nat. Mater.* **2014**, *13*, 586.
[45] T. Ohzuku, M. Kitagawa, T. Hirai, *J. Electrochem. Soc.* **1990**, *137*, 769.
[46] D. Qian, B. Xu, M. Chi, Y. S. Meng, *Phys. Chem. Chem. Phys.* **2014**, *16*, 14665.
[47] Y. Kan, Y. Hu, C. K. Lin, Y. Ren, Y. K. Sun, K. Amine, Z. Chen, *Phys. Chem. Chem. Phys.* **2014**, *16*, 20697.
[48] K. S. Kang, Y. S. Meng, J. Breger, C. P. Grey, G. Ceder, *Science* **2006**, *311*, 977.
[49] C. Delmas, J. P. Pérès, A. Rougier, A. Demourgues, F. Weill, A. Chadwick, M. Broussely, F. Perton, P. Biensan, P. Willmann, *J. Power Sources* **1997**, *68*, 120.
[50] P. F. Yan, J. M. Zheng, D. P. Lv, Y. Wei, J. X. Zheng, Z. G. Wang, S. Kuppan, J. G. Yu, L. L. Luo, D. Edwards, M. Olszta, K. Amine, J. Liu, J. Xiao, F. Pan, G. Y. Chen, J. G. Zhang, C. M. Wang, *Chem. Mater.* **2015**, *27*, 5393.
[51] G. Chen, B. Hai, A. K. Shukla, H. Duncan, *J. Electrochem. Soc.* **2012**, *159*, A1543.

